Peiman Naseradinmousavi
Assistant Professor
Department of Mechanical Engineering,
San Diego State University,
San Diego, CA 92115
e-mail: pnaseradinmousavi@mail.sdsu.edu;
peiman.n.mousavi@gmail.com

Miroslav Krstić
Daniel L. Alspach Endowed Chair in Dynamic Systems and Control,
Department of Mechanical and Aerospace Engineering,
University of California, San Diego,
San Diego, CA 92093
e-mail: krstic@ucsd.edu

C. Nataraj
Mr. & Mrs. Robert F. Moritz, Sr. Endowed Chair Professor in Engineered Systems,
Department of Mechanical Engineering,
Villanova University,
Villanova, PA 19085
e-mail: nataraj@villanova.edu

Design Optimization of Dynamically Coupled Actuated Butterfly Valves Subject to a Sudden Contraction

In this effort, we present novel nonlinear modeling of two solenoid actuated butterfly valves subject to a sudden contraction and then develop an optimal configuration in the presence of highly coupled nonlinear dynamics. The valves are used in the so-called smart systems employed in a wide range of applications including bioengineering, medicine, and engineering fields. Typically, thousands of the actuated valves operate together to regulate the amount of flow and also to avoid probable catastrophic disasters which have been observed in practice. We focus on minimizing the amount of energy used in the system as one of the most critical design criteria to yield an efficient operation. We optimize the actuation subsystems interacting with the highly nonlinear flow loads in order to minimize the amount of energy consumed. The contribution of this work is the inclusion of coupled nonlinearities of electromechanical valve systems to optimize the actuation units. Stochastic, heuristic, and gradient based algorithms are utilized in seeking the optimal design of two sets. The results indicate that substantial amount of energy can be saved by an intelligent design that helps select parameters carefully and also uses flow torques to augment the closing efforts. [DOI: 10.1115/1.4032215]

1 Introduction

Generally smart systems have received much attention for a wide range of applications to be operated efficiently with respect to the amount of energy used in the actuator units. The U.S. Navy has particularly focused on developing reliable and energy efficient systems to minimize the cost of operation and also to increase crew safety through a stable performance.

Automation systems typically consist of actuators, sensors, controllers, valves, piping, electrical cabling, and communication wiring. Many types of actuator-valve systems are in use [1,2]. One of the most critical systems to be utilized in cooling purposes is the so-called smart valve system. The main objective of the smart valves is to shut down automatically in case of breakage and to reroute the flow as needed.

These sets include many interdisciplinary components interacting with each other through highly coupled nonlinear dynamics. We have previously analyzed a solenoid actuated butterfly valve dealing with electromagnetics and fluid mechanics [3–6]. High fidelity mathematical models were developed for both the single and coupled actuated valves. For the single set [3], our focus was on developing a nonlinear model to analyze the complicated physics of the system to be used in dynamic analysis [4] and optimization [5].

We have captured transient chaotic and crisis dynamics of the single valve actuator for some critical parameters helping to define safe domains of operation. Determining the safe operational domain through the stability map helped us define the lower and upper bounds of the optimization tasks [5] and operation, which reduced the amount of energy used in the single set. The first phase was to optimize the system design, particularly the actuation unit coupled with the mechanical and fluid parts. We then optimized the valve operation to be closed in an efficient fashion yielding the minimum energy consumption. In both the optimization schemes, the roles of flow torques are important to help close the valve with minimal energy.

Contributed by the Design Automation Committee of ASME for publication in the Journal of Mechanical Design. Manuscript received June 28, 2015; final manuscript received December 1, 2015; published online February 19, 2016. Assoc. Editor: Ettore Pennestri.

It is of great interest to emphasize that the smart valve systems contain many of the actuated sets, and hence, they would not be independent of each other. These dependencies have been observed in practice and probable malfunction of each set may expectedly result in the catastrophic behavior of the whole system. Therefore, we have developed the coupled dynamic model of two actuated valves operating in series [6]. A periodic noise was applied on the upstream valve to evaluate its effects on the downstream set of the valve and actuator. A powerful tool of the nonlinear dynamic analysis (power spectrum) was then employed to present the same oscillatory response of the downstream set with that of the upstream one; as expected, the downstream set revealed the same frequencies of response with a smaller amplitude. Any slight dynamic change of the upstream set, on the other hand, was shown to be effective for the downstream set through the media trapped between two valves.

Capturing the coupled dynamics of two actuated valves would help us optimize the design of both the actuation units in which an interesting connection can be distinguished between the currents. The currents are subject to the interconnected flow torques and pressure drops of the valves. Note that, for the single set, we neglected the interactions among the actuators/valves operating in series although the magnetic parts are remarkably affected by the dynamics of the neighbor sets [6].

Important nonlinear phenomena in electromechanical systems have also received considerable attention. Belato et al. [7] analyzed chaotic vibrations of an electromechanical system which includes a nonlinear dynamic system consisting of a simple pendulum whose support point is vibrated along a horizontal guide by a two-bar linkage driven by a DC motor with limited power. Nonlinear dynamic analysis of a micro-electromechanical system (MEMS) has been carried out by Xie et al. [8] based on an invariant manifold method proposed by Boivin et al. [9]. Ge and Lin [10] have studied dynamical analysis of an electromechanical gyrostat system subjected to an external disturbance.

Optimization of solenoid actuators has recently received some attention. Baek-Ju and Eun-Woong [11] have focused on the optimal design of solenoid actuators using a nonmagnetic ring. Electromagnetic actuator-current development has been carried out by Hameyer and Nienhaus [12], and Sung et al. [13] studied the

 Copyright © 2016 by ASME

Downloaded From: http://mechanicaldesign.asmedigitalcollection.asme.org/ on 02/19/2016 Terms of Use: http://www.asme.org/about-asme/terms-of-use

development of a design process for on-off type of solenoid actuators. Kajima [14] has considered a dynamic model of the plunger type of solenoids. Karr and Scott [15] utilized the genetic algorithm to optimize an antiresonant electromechanical controller operating in a frequency domain. Mahdi [16] carried out optimization of the PID controller parameters to operate nonlinear electromechanical actuator efficiently. A coupled electromechanical optimization of the cost of high speed railway overheads has been carried out by Jimenez-Octavio et al. [17]. Nowak [18] has focused on presenting an algorithm of the optimization of the dynamic parameters of an electromagnetic linear actuator operating in error-actuated control system. Other contributions in design optimization of electromechanical actuators include Refs. [19–25].

This paper begins with a brief nonlinear dynamic model of the actuators/valves operating in series but is somewhat different from the model reported in Ref. [6] due to the sudden contraction. In practice, multiple contractions and expansions exist through the pipeline. The coupled modeling and then analysis of these configurations would hence be necessary to capture highly nonlinear mutual interactions among the sets. Then, the optimal design process is formulated to help select the appropriate actuator parameters coupled with the electromagnetical, mechanical, and fluid parts in order to yield an energy efficient system. Most electromechanical systems used in the flow control lines have been studied by neglecting the interconnections imposed by other sets. From another aspect, the linearization method, as one of the simplest practices, is widely being utilized in many of analytical investigations particularly for systems with a higher level of complexity and coupling. The results of both the isolated and linearized analyses may expectedly be valid within a narrow domain of operation leading typically to significant inaccuracy and unreliability of the results. The contribution of this work is to optimize both the actuated valves dynamically coupled in different aspects while our previous effort [5] was on optimizing a single unit by neglecting its dynamic coupling with another set. A considerable amount of energy saving was obtained via the isolated analysis but would obviously could be affected by the dynamic interactions among sets. In this effort, a lumped cost function will be minimized, with respect to the stability and physical constraints, using global optimization tools in order to obtain efficient design and operation of the actuation units and valves, respectively. This would provide an interesting opportunity to utilize the coupled optimization scheme, which is being developed here, for other large-scale networks including oil and gas fields, municipal piping systems, petrochemical plants, and aerospace. The need for optimization clearly exists for such networks in order to improve efficiency.

2 Mathematical Modeling

The system being optimized consists of two solenoid actuated butterfly valves operating in series as shown in Fig. 1(*a*). The actuators are connected to the valve stems through rack and pinion arrangements. Applying electric voltages (AC or DC), the magnetic forces move the plungers and consequently rotate both the valves to desirable angles. Note that we utilize a return spring to open the valves; this is a common practice among manufacturers.

The mathematical modeling of such a coupled system obviously needs some simplifying assumptions to avoid useless and cumbersome numerical calculations. The first one is to neglect magnetic diffusion. During the diffusion time, there is no powerful magnetic force to move the plunger and the valve subsequently would not rotate in that time interval. Note that the diffusion time has an inverse relationship with the amount of current [3] such that a large value of the current yields a negligible diffusion time and vice versa. We apply a current of $i = 13.3$ (A) for both the actuators yielding the diffusion time of $\tau_d \approx 6\,(\mathrm{ms})$ which can be easily neglected considering the nominal operation time.

The second assumption is to utilize laminar flow for both the valves. This is a common practice to avoid the tedious numerical calculations of a turbulent regime and also to develop an analytical model to be used in the nonlinear dynamic analysis. The dynamic analysis needs to be done to capture the dangerous responses of the system [4]. The validity of laminar flow assumption needs to be examined particularly with respect to the amounts of inlet velocity and pipe diameter given in Table 1. Using these values, the Reynolds number indicates the existence of the turbulent regime and questions the assumption of laminar flow. We hence carried out the experimental work shown in Fig. 2 to examine the validity of the assumption. Note that the flow loads including hydrodynamic and bearing ones are the most important torques affecting the valves' and actuators' interconnected dynamics. The analytical formulas developed for both the torques have been based on the assumption of laminar flow. We have therefore carried out the experimental work in order to examine the accuracy of the torques' mathematical formulas developed for a symmetric valve. Figure 3 shows the total torque, which is the sum of both the hydrodynamic and bearing ones, for the inlet velocity of $v \approx 2.7(\mathrm{m/s})$ and valve diameter of $D_v = 2\,(\mathrm{in.})$ revealing an acceptable consistency [26] among the experimental data and the formula utilized in the analytical studies based on the laminar flow. This also gives us the confidence to use the analytically (and computationally) derived mathematical expressions for the hydrodynamic and bearing torques. We previously discussed the important roles of both the torques on the dynamic response of a single actuated valve and subsequently such effects are expected to be observed for the coupled sets [6].

We modeled the coupled system as two changing resistors for the opening/closing valves plus three constant ones in the middle of the valves, shown in Fig. 1(*b*). Two of the constant resistors stand for head losses and another one is due to the sudden contraction. The inlet and outlet pressures are supposed to be known. Applying the assumption stated for the dominant laminar flow, the Hagen–Poiseuille [27] and Borda–Carnot [28] formulas express the pressure drops between two valves (points 1 and 2)

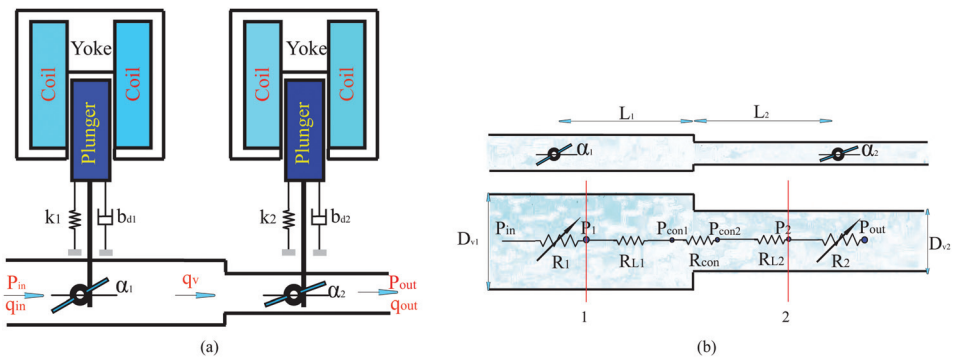

Fig. 1 (*a*) Two actuated butterfly valves subject to the sudden contraction and (*b*) a model of two valves in series without actuation

Downloaded From: http://mechanicaldesign.asmedigitalcollection.asme.org/ on 02/19/2016 Terms of Use: http://www.asme.org/about-asme/terms-of-use

Table 1 The system parameters

ρ	$1000(\mathrm{kg/m^3})$	v	$3(\mathrm{m/s})$
μ	0.5	P_{in}	256 (kPa)
$J_{1,2}$	0.104×10^{-1} (kg m^2)	$b_{d1,d2}$	$6420 \frac{\mathrm{N \cdot m \, s}}{\mathrm{rad}}$
N_1	3000	$C_{11,22}$	$1.56 \times 10^6(\mathrm{H^{-1}})$
$g_{m1,m2}$	0.1 (m)	$V_{1,2}$	24 (V)
D_{v1}	0.2032 (m)	D_{v2}	0.127 (m)
$D_{s1,s2}$	0.01 (m)	P_{out}	2 (kPa)
$k_{1,2}$	$60(\mathrm{N \cdot m^{-1}})$	$C_{21,22}$	$6.32 \times 10^8(\mathrm{H^{-1}})$
L_1	2 (m)	L_2	1 (m)
μ_f	0.018 (kg m^{-1} s^{-1})	$R_{1,2}$	1.8 (Ω)
$r_{1,2}$	0.05 (m)	θ	90deg
N_2	3000		

$$P_1 - P_{\text{con1}} = \underbrace{\frac{128\mu_f L_1}{\pi D_{v1}^4}}_{R_{L1}} q_v \tag{1}$$

$$P_{\text{con1}} - P_{\text{con2}} = \frac{1}{2} K_{\text{con}} \rho v_{\text{out}}^2 \tag{2}$$

$$P_{\text{con2}} - P_2 = \underbrace{\frac{128\mu_f L_2}{\pi D_{v2}^4}}_{R_{L2}} q_v \tag{3}$$

where μ_f is the fluid dynamic viscosity, D_{v1} and D_{v2} stand for the valves' diameters, q_v indicates the volumetric flow rate, L_1 and L_2 are the pipe lengths before and after contraction, P_{con1} and P_{con2} indicate the flow pressures before and after contraction, and R_{L1} and R_{L2} are the constant resistances. K_{con} is easily calculated as follows:

$$K_{\text{con}} = 0.5\left(1 - \beta^2\right)\sqrt{\sin\left(\frac{\theta}{2}\right)} \tag{4}$$

where θ is the angle of approach and β indicates the ratio of minor and major diameters (D_{v2}/D_{v1}). Using the parameters given in Table 1, we obtain $K_{\text{con}} = 0.2562$. We rewrite Eq. (2) as the following:

$$P_{\text{con1}} - P_{\text{con2}} = \frac{1}{2} K_{\text{con}} \rho v_{\text{out}}^2 = \underbrace{\frac{8K_{\text{con}}}{\pi^2 D_{v2}^4}\rho}_{R_{\text{con}}} \underbrace{\frac{\pi^2 D_{v2}^4 v_{\text{out}}^2}{16}}_{q_v^2} = R_{\text{con}} q_v^2 \tag{5}$$

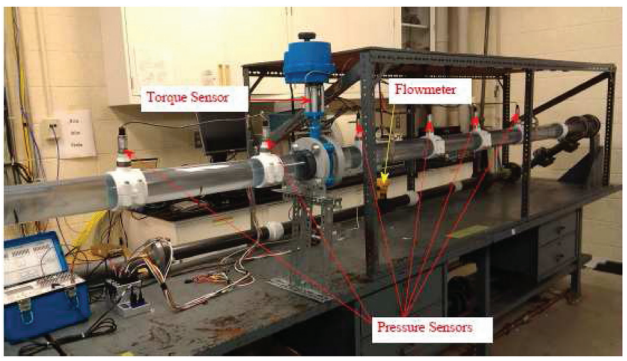

Fig. 2 The experimental work carried out for a single set

where R_{con} is the resistance due to the sudden contraction. Adding Eqs. (1)–(3) and (5) easily yields

$$P_1 - P_2 = [R_{L1} + R_{L2} + R_{\text{con}} q_v] q_v \tag{6}$$

The valve's "resistance (R)" and "coefficient (c_v)" are the most important parameters of the regulating valves including butterfly ones. The valve's resistance and coefficient are nonlinear functions of the valve rotation angle [29]

$$R_i(\alpha_i) = \frac{891 D_{vi}^4}{c_{vi}^2(\alpha_i)}, \; i = 1, 2 \tag{7}$$

The pressure drop across the valve is stated as follows [30]:

$$\Delta P_i(\alpha_i) = 0.5 R_i(\alpha_i) \rho v^2 \tag{8}$$

where α indicates the valve rotation angle, v is the flow velocity, and ρ stands for the density of the media. Rewriting Eq. (8) yields

$$\Delta P_i(\alpha_i) = \underbrace{\frac{\pi^2 D_{vi}^4 v^2}{16}}_{q_v^2} \underbrace{\frac{8 \times R_i(\alpha_i)\rho}{\pi^2 D_{vi}^4}}_{R_{ni}(\alpha_i)} = R_{ni}(\alpha_i) q_v^2 \tag{9}$$

We established that both the hydrodynamic (T_h) and bearing (T_b) torques [30,31] are too sensitive to the pressure drop obtained via Eq. (9) leading us to reformulate them to be stated as follows:

$$f_i(\alpha_i) = \frac{16 T_{ci}(\alpha_i)}{3\pi\left(1 - \frac{C_{cci}(\alpha_i)\left(1 - \sin(\alpha_i)\right)}{2}\right)^2} \tag{10}$$

$$T_{hi} = \frac{16 T_{ci}(\alpha_i) D_{vi}^3 \Delta P_i}{3\pi\left(1 - \frac{C_{cci}(\alpha_i)\left(1 - \sin(\alpha_i)\right)}{2}\right)^2} = f_i(\alpha_i) D_{vi}^3 \Delta P_i \tag{11}$$

$$T_{bi} = 0.5 A_d \Delta P_i \mu D_s = C_i \Delta P_i \tag{12}$$

where μ is the friction coefficient of the bearing area, D_s indicates the stem diameter of the valve, $C_i = (\pi/8)\mu D_{vi}^2 D_s$, and T_{ci} and C_{cci} stand for the hydrodynamic torque and the sum of upper and lower contraction coefficients, respectively; they depend on the valve rotation angle [3].

The nonlinear dynamic analysis carried out for a set of the actuator/valve [4] provides the criteria needed to determine the bounds of the optimization tasks; the stability analysis obviously needs to

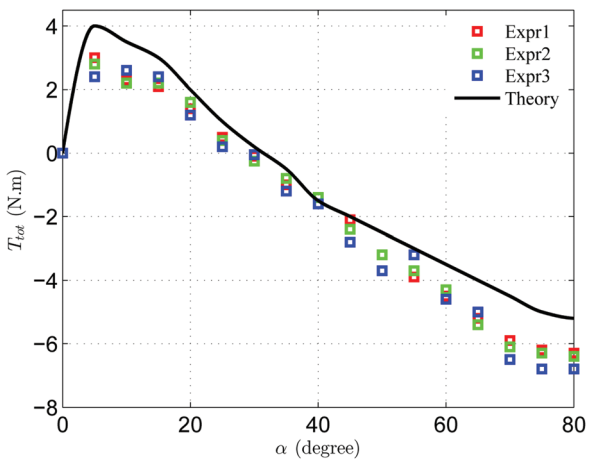

Fig. 3 The experimental and analytical total torques for the inlet velocity of $v \approx 2.7(\mathrm{m/s})$ and valve diameter of $D_v = 2$ (in.)

Downloaded From: http://mechanicaldesign.asmedigitalcollection.asme.org/ on 02/19/2016 Terms of Use: http://www.asme.org/about-asme/terms-of-use

be done using an analytical model. We would utilize the same practice for the coupled system with the aid of fitting suitable curves on c_{vi} and R_{ni} in order to model the system analytically. For our case study of $D_{v1} = 8$ (in.) and $D_{v2} = 5$ (in.), the valves' coefficients and resistances are formulated as follows:

$$c_{v1}(\alpha_1) = p_1\alpha_1^3 + q_1\alpha_1^2 + o_1\alpha_1 + s_1 \tag{13}$$

$$c_{v2}(\alpha_2) = p_2\alpha_2^3 + q_2\alpha_2^2 + o_2\alpha_2 + s_2 \tag{14}$$

$$R_{n1}(\alpha_1) = \frac{e_1}{\left(p_1\alpha_1^3 + q_1\alpha_1^2 + o_1\alpha_1 + s_1\right)^2} \tag{15}$$

$$R_{n2}(\alpha_2) = \frac{e_2}{\left(p_2\alpha_2^3 + q_2\alpha_2^2 + o_2\alpha_2 + s_2\right)^2} \tag{16}$$

where $e_1 = 7.2 \times 10^5$, $e_2 = 4.51 \times 10^5$, $p_1 = 461.9$, $p_2 = 161.84$, $q_1 = -405.4$, $q_2 = -110.53$, $o_1 = -1831$, $o_2 = -695.1$, $s_1 = 2207$, and $s_2 = 807.57$. Note that the curves were selected based on the decremental and incremental profiles of the valves' coefficients and resistances, respectively, in which we have reported in Refs. [6] and [26]. Clearly the mass continuity principle implies $q_{\text{in}} = q_{\text{out}} = q_v$. Rewriting Eq. (9) then yields

$$\frac{P_{\text{in}} - P_1}{R_{n1}(\alpha_1)} = \frac{P_2 - P_{\text{out}}}{R_{n2}(\alpha_2)} \tag{17}$$

$$R_{n1}P_2 + R_{n2}P_1 = R_{n2}P_{\text{in}} + R_{n1}P_{\text{out}} \tag{18}$$

One can easily derive the coupled P_1 and P_2 terms by combining Eqs. (6) and (18) as follows:

$$P_1 = \frac{R_{n2}P_{\text{in}} + R_{n1}P_{\text{out}} + R_{n1}(R_{L1} + R_{L2} + R_{\text{con}}q_v)q_v}{(R_{n1} + R_{n2})} \tag{19}$$

$$P_2 = \frac{R_{n2}P_{\text{in}} + R_{n1}P_{\text{out}} - R_{n2}(R_{L1} + R_{L2} + R_{\text{con}}q_v)q_v}{(R_{n1} + R_{n2})} \tag{20}$$

Equations (19) and (20) state the roles of R_{n1}, R_{n2}, R_{L1}, R_{L2}, and R_{con} on the variations of P_1 and P_2 with the given values of P_{in}, P_{out}, and q_v, as observed in the practice. Therefore, it is fairly straightforward to determine the dynamic sensitivity of the downstream set to any slight changes of the upstream one. We then can rewrite both the hydrodynamic and bearing torques dependency on all the resistances as follows:

$$T_{hi} = f_i(\alpha_i)D_{vi}^3\Delta P_i(R_{n1}, R_{n2}, R_{L1}, R_{L2}, R_{\text{con}}) \tag{21}$$

$$T_{bi} = C_i\Delta P_i(R_{n1}, R_{n2}, R_{L1}, R_{L2}, R_{\text{con}}) \tag{22}$$

Note that f_i is a function of many nonlinear terms which include the changing T_{ci} and C_{cci} in addition to the valve angles. For a systematic analysis of the whole system, the following functions are fitted to the $D_{vi}^3 f_i$ of each valve [6,26]:

$$\begin{aligned} T_{h1} &= \underbrace{\left(a_1\alpha_1 e^{b_1\alpha_1^{1.1}} - c_1 e^{d_1\alpha_1}\right)}_{D_{v1}^3 f_1}(P_{\text{in}} - P_1) \\ &= \left(a_1\alpha_1 e^{b_1\alpha_1^{1.1}} - c_1 e^{d_1\alpha_1}\right) \times \frac{e_1}{\left(p_1\alpha_1^3 + q_1\alpha_1^2 + o_1\alpha_1 + s_1\right)^2} \\ &\quad \times \frac{}{\sum_{i=1}^{2} \frac{e_i}{\left(p_i\alpha_i^3 + q_i\alpha_i^2 + o_i\alpha_i + s_i\right)^2}} \\ &\quad \times (P_{\text{in}} - P_{\text{out}} - (R_{L1} + R_{L2} + R_{\text{con}}q_v)q_v) \end{aligned} \tag{23}$$

$$\begin{aligned} T_{h2} &= \underbrace{\left(a_1'\alpha_2 e^{b_1'\alpha_2^{1.1}} - c_1' e^{d_1'\alpha_2}\right)}_{D_{v2}^3 f_2}(P_2 - P_{\text{out}}) \\ &= \left(a_1'\alpha_2 e^{b_1'\alpha_2^{1.1}} - c_1' e^{d_1'\alpha_2}\right) \times \frac{e_2}{\left(p_2\alpha_2^3 + q_2\alpha_2^2 + o_2\alpha_2 + s_2\right)^2} \\ &\quad \times \frac{}{\sum_{i=1}^{2} \frac{e_i}{\left(p_i\alpha_i^3 + q_i\alpha_i^2 + o_i\alpha_i + s_i\right)^2}} \\ &\quad \times (P_{\text{in}} - P_{\text{out}} - (R_{L1} + R_{L2} + R_{\text{con}}q_v)q_v) \end{aligned} \tag{24}$$

where $a_1 = 0.4249$, $a_1' = 0.1022$, $b_1 = -18.52$, $b_1' = -17.0795$, $c_1 = -7.823 \times 10^{-4}$, $c_1' = -2 \times 10^{-4}$, $d_1 = -1.084$, and $d_1' = -1.0973$. We also replace the sign function ($\text{sign}(\dot{\alpha}_i)$), which is being used in the bearing torque statement to present its resistance role, by the smooth function $\tanh(K\dot{\alpha}_i)$ for ease of analysis. Figures 4(*a*) and 4(*b*) are the results of the stability analysis of the coupled system; we will report this effort as another article.

The state variables are defined as follows:

$$[z_1, z_2, z_3, z_4, z_5, z_6] = [\alpha_1, \dot{\alpha}_1, i_1, \alpha_2, \dot{\alpha}_2, i_2]$$

where $z_1 = \alpha_1$, $z_2 = \dot{\alpha}_1$, and $z_3 = i_1$ stand for the upstream valve's rotation angle, angular velocity, and actuator current, respectively. $z_4 = \alpha_2$, $z_5 = \dot{\alpha}_2$, and $z_6 = i_2$ indicate the downstream valve's rotation angle, angular velocity, and actuator current, respectively. We have previously developed the magnetic force and rate of current terms [3] which are used in deriving the state space equations as follows:

$$F_{mi} = \frac{C_{2i}N_i^2 i_i^2}{2\left(C_{1i} + C_{2i}(g_{mi} - x_i)\right)^2} \tag{25}$$

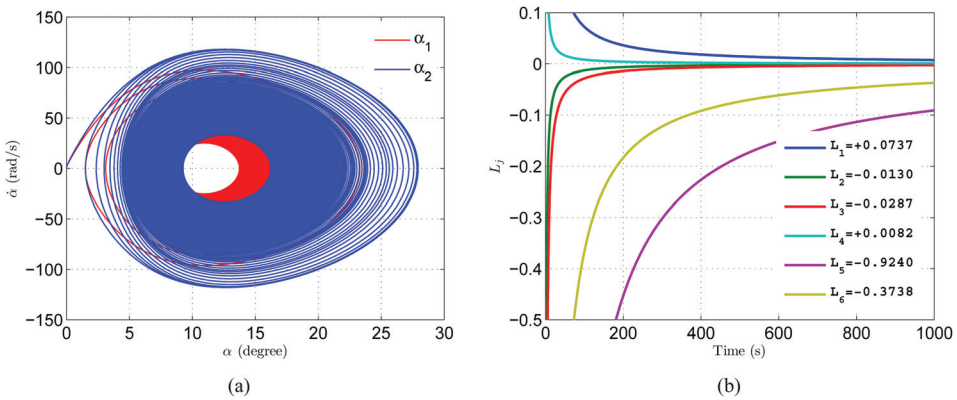

(a) (b)

Fig. 4 (*a*) Chaotic dynamics of the valves/actuators and (*b*) Lyapunov exponents indicating the chaotic dynamics of the system

Downloaded From: http://mechanicaldesign.asmedigitalcollection.asme.org/ on 02/19/2016 Terms of Use: http://www.asme.org/about-asme/terms-of-use

$$\frac{di_i}{dt} = \frac{(V_i - R_i i_i)\left(C_{1i} + C_{2i}(g_{mi} - x_i)\right)}{N_i^2} - \frac{C_{2i} i_i \dot{x}_i}{\left(C_{1i} + C_{2i}(g_{mi} - x_i)\right)} \tag{26}$$

$$\dot{z}_1 = z_2 \tag{27}$$

$$\dot{z}_2 = \frac{1}{J_1}\left[\frac{r_1 C_{21} N_1^2 z_3^2}{2\left(C_{11} + C_{21}(g_{m1} - r_1 z_1)\right)^2} - b_{d1} z_2 - k_1 z_1 + \frac{\dfrac{(P_{\text{in}} - P_{\text{out}} - (R_{L1} + R_{L2} + R_{\text{con}} q_v) q_v) e_1}{\left(p_1 z_1^3 + q_1 z_1^2 + o_1 z_1 + s_1\right)^2}}{\sum_{i=1,4} \dfrac{e_i}{\left(p_i z_i^3 + q_i z_i^2 + o_i z_i + s_i\right)^2}} \times \left[\left(a_1 z_1 e^{b_1 z_1^{1.1}} - c_1 e^{d_1 z_1}\right) - C_1 \times \tanh(K z_2)\right]\right] \tag{28}$$

$$\dot{z}_3 = \frac{(V_1 - R_1 z_3)\left(C_{11} + C_{21}(g_{m1} - r_1 z_1)\right)}{N_1^2} - \frac{r_1 C_{21} z_3 z_2}{\left(C_{11} + C_{21}(g_{m1} - r_1 z_1)\right)} \tag{29}$$

$$\dot{z}_4 = z_5 \tag{30}$$

$$\dot{z}_5 = \frac{1}{J_2}\left[\frac{r_2 C_{22} N_2^2 z_6^2}{2\left(C_{12} + C_{22}(g_{m2} - r_2 z_4)\right)^2} - b_{d2} z_5 - k_2 z_4 + \frac{\dfrac{(P_{\text{in}} - P_{\text{out}} - (R_{L1} + R_{L2} + R_{\text{con}} q_v) q_v) e_2}{\left(p_2 z_4^3 + q_2 z_4^2 + o_2 z_4 + s_2\right)^2}}{\sum_{i=1,4} \dfrac{e_i}{\left(p_i z_i^3 + q_i z_i^2 + o_i z_i + s_i\right)^2}} \times \left[\left(a_1' z_4 e^{b_1' z_4^{1.1}} - c_1' e^{d_1' z_4}\right) - C_2 \times \tanh(K z_5)\right]\right] \tag{31}$$

$$\dot{z}_6 = \frac{(V_2 - R_2 z_6)\left(C_{12} + C_{22}(g_{m2} - r_2 z_4)\right)}{N_2^2} - \frac{r_2 C_{22} z_5 z_6}{\left(C_{12} + C_{22}(g_{m2} - r_2 z_4)\right)} \tag{32}$$

where x indicates the plunger displacement, r is the radius of the pinion, F_m stands for the motive force, C_1 and C_2 are the reluctances of the magnetic path without air gap and that of the air gap, respectively, N is the number of coils, i indicates the applied current, g_m is the nominal airgap, J is the polar moment of inertia of the valve's disk, b_d is the equivalent torsional damping, K_t indicates the equivalent torsional stiffness, V is the supply voltage, and R indicates the electrical resistance of coil. Note that $K = 1$ resulted in a good approximation to the sign function. Equations (27)–(32) constitute the sixth order dynamic model of the coupled actuators/valves. Figure 5 is a block diagram of the interconnected sets to simply visualize Eqs. (27)–(32). Note that the analytical model would not be valid at $z_1 = 90$deg and $z_4 = 90$deg [3–6,30].

3 Optimal Design

Efficient optimization schemes are needed to be utilized in minimizing the amount of energy used by the whole system with respect to the stability criteria we have reported earlier [4,32]. Neglecting the parameter constraints established through the stability analysis would result in the failure of the whole system shown in Fig. 4(*a*) revealing the chaotic dynamics of both the valves/actuators for a set of critical parameters; two positive Lyapunov exponents shown in Fig. 4(*b*) confirm the chaotic behavior of the system. Some critical values of the equivalent viscous damping and friction coefficient of the bearing area ($b_{di} = 10^{-3}$, $\mu_i = 5 \times 10^{-2}$) lead to chaotic behavior, the details of which will be presented as another article.

The problem is one of constrained optimization with possibly several local minima. Therefore, we need to utilize efficient optimization approaches to obtain the global minimum; the constraints are the stability and physical ones. The cost function we wish to minimize is a sum of the energy used in both the sets

$$\min E_{\text{tot}} = \sum_{i=1}^{2} \int_0^{t_f} V i_i \, dt$$
$$\text{subject to : } z_1 < 90\,\text{deg},\ z_4 < 90\,\text{deg} \tag{33}$$

The cost function is typically determined with respect to the scale and performance of the network. Thousands of such actuated valves are used in the U.S. Navy fleet and a lower lumped amount of energy consumed in the network is needed to reduce the cost of operation. This would lead us to select a lumped cost function to be minimized. After selecting some of the parameters as predetermined, the design variables to be used in the optimization process are chosen as follows: C_{11}, C_{12}, C_{21}, and C_{22} are the magnetic reluctances, g_{m1} and g_{m2} indicate the airgaps, and N_1 and N_2 are the number of coils for both the actuators. We next collect the design variables into a vector

Downloaded From: http://mechanicaldesign.asmedigitalcollection.asme.org/ on 02/19/2016 Terms of Use: http://www.asme.org/about-asme/terms-of-use

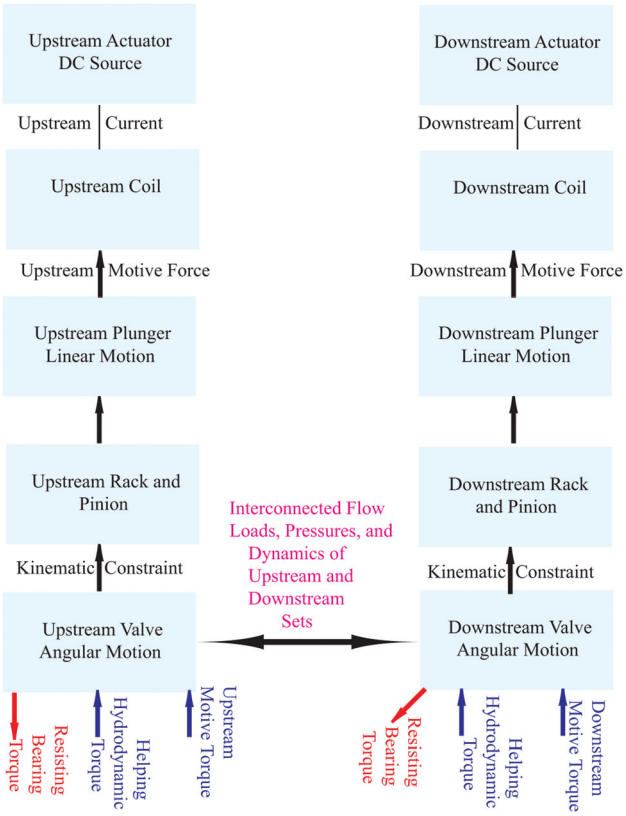

Fig. 5 The block diagram of the interconnected sets

$$\theta_1 = [C_{11}, C_{12}, C_{21}, C_{22}, N_1, N_2, g_{m1}, g_{m2}]^{\mathrm{T}} \tag{34}$$

The state equations, as discussed earlier, need to be satisfied at all times during the optimization process and the design variables are subject to the following lower and upper bounds:

$$\theta_{1\min} = [0.6{*}10^6, 0.6{*}10^6, 3{*}10^8, 3{*}10^8, 3000, 3000, 0.065, 0.065]^{\mathrm{T}} \tag{35}$$

$$\theta_{1\max} = [1.6{*}10^6, 1.6{*}10^6, 6.5{*}10^8, 6.5{*}10^8, 3600, 3600, 0.11, 0.11]^{\mathrm{T}} \tag{36}$$

These bounds were established based on practical system considerations, stability analysis [4,26], and physical constraints. We employ three global optimization tools including simulated annealing (SA), genetic (GA), and gradient based algorithms to provide a clear map of optimization efforts with respect to the locality/globality of the cost function minima. SA was independently developed by Kirkpatrick et al. [33] and by Cerny [34]. Genetic optimization has been designed based on a heuristic search to mimic the process of natural selection [35].

The design variables in practice are not of the same order, and caused serious numerical errors in our initial studies. We solved this issue by conditioning them using a normalization scheme as follows:

$$N_{ni} = \frac{N_i}{10^3};\ C_{1\text{in}} = \frac{C_{1i}}{10^6};\ C_{2\text{in}} = \frac{C_{2i}}{10^8};\ g_{\min} = 10 g_{mi}$$

One of the advantages of the SA procedure is to select a new point randomly. We hence need to set the initial guesses as random numbers. The algorithm covers all new points to reduce the value of the objective function. At the same time, with a certain probability, points that increase the objective function are also accepted. The algorithm avoids being trapped in local minima by using points that raise the objective function value and has the potential to search globally for more possible solutions.

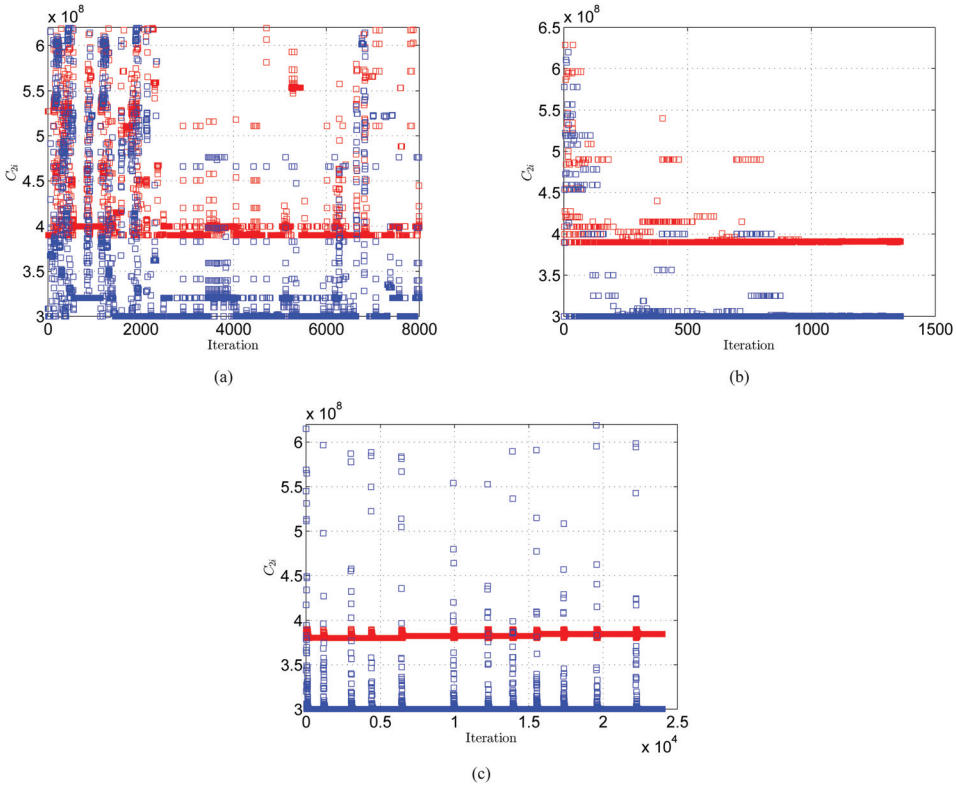

Fig. 6 The optimized C_{2i} ; red and blue squares stand for the upstream and downstream sets, respectively: (*a*) GS, (*b*) GA, and (*c*) SA

Downloaded From: http://mechanicaldesign.asmedigitalcollection.asme.org/ on 02/19/2016 Terms of Use: http://www.asme.org/about-asme/terms-of-use

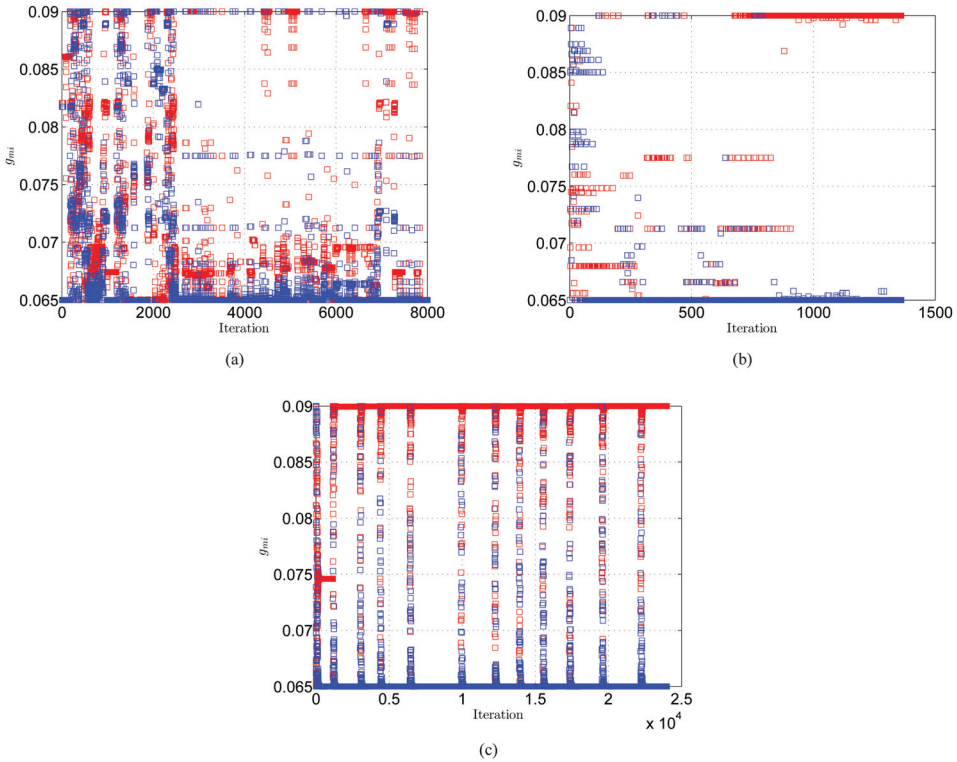

Fig. 7 The optimized g_m: (*a*) GS, (*b*) GA, and (*c*) SA

The genetic algorithm is significantly more robust than other conventional ones. It does not break down easily in the presence of slight changes of inputs, and noise. For a large state-space, the algorithm may potentially exhibit significantly better performance than typical optimization techniques.

The random initial guesses we used in the optimization process (as required by SA) are as follows:

$$\theta_{nr} = \theta_{lb} + (\theta_{ub} - \theta_{lb}) \times \text{rand}(0, 1) \tag{37}$$

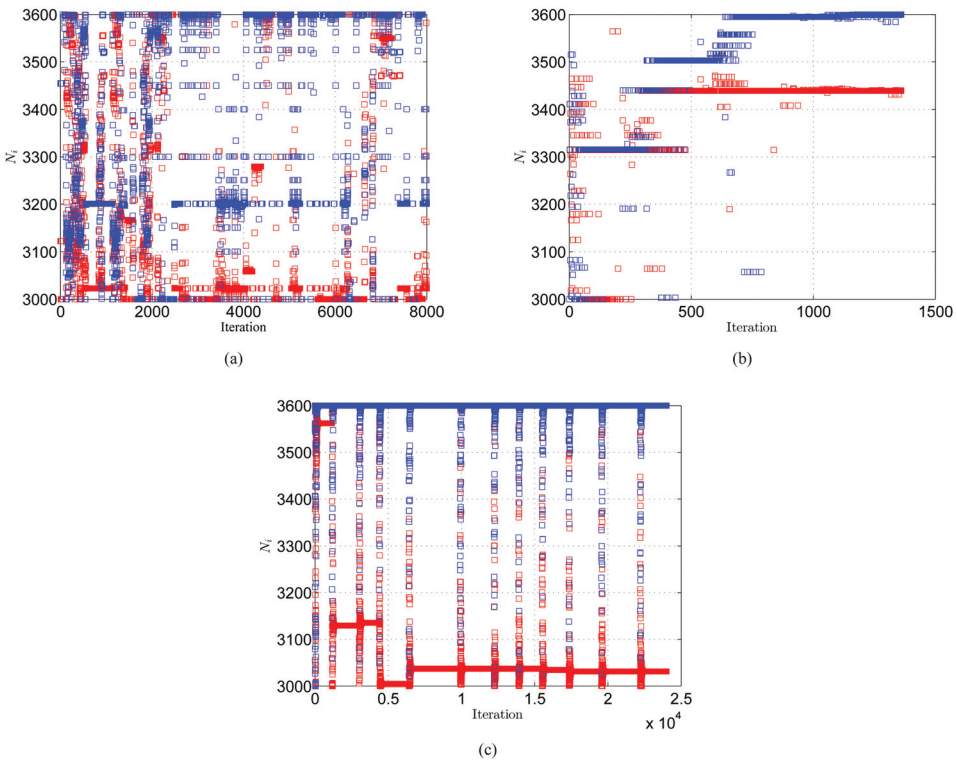

Fig. 8 The optimized *N*: (*a*) GS, (*b*) GA, and (*c*) SA

Downloaded From: http://mechanicaldesign.asmedigitalcollection.asme.org/ on 02/19/2016 Terms of Use: http://www.asme.org/about-asme/terms-of-use

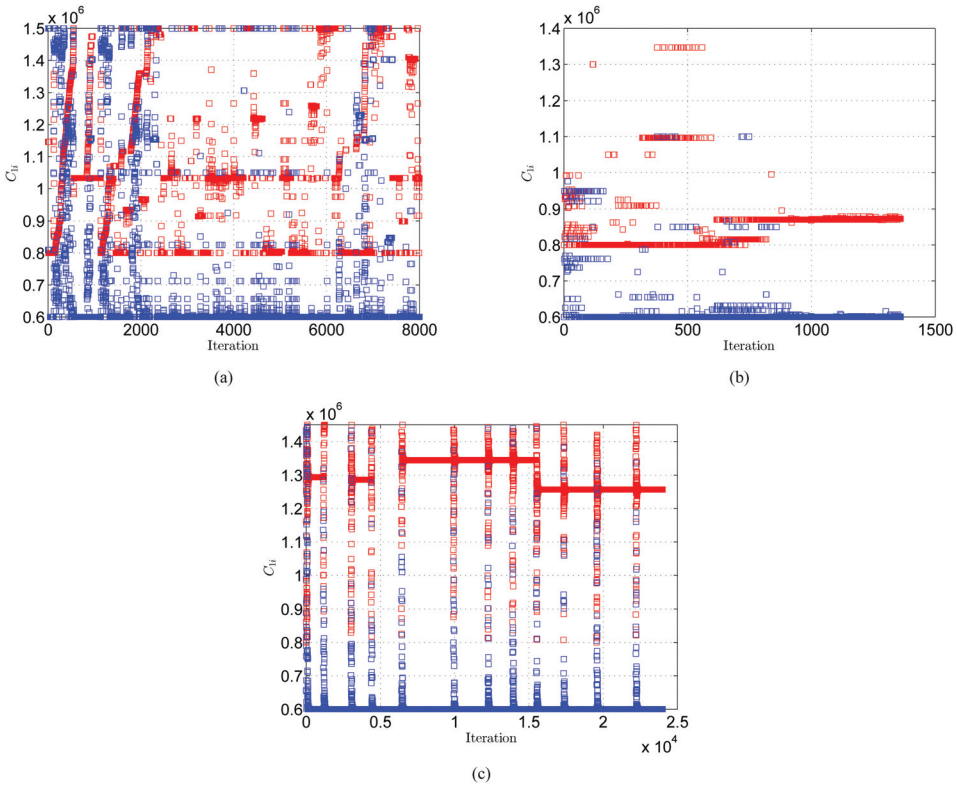

Fig. 9 The optimized C_{1i} : (*a*) GS, (*b*) GA, and (*c*) SA

Table 2 The nominal and optimal variables

	Nominal	GS	GA	SA
g_{m1} (m)	0.1	0.09	0.09	0.09
g_{m2} (m)	0.1	0.065	0.065	0.065
$\frac{C_{21}}{10^8}$ (H^{-1})	6.32	3.9	3.9	3.9
$\frac{C_{22}}{10^8}$ (H^{-1})	6.32	3	3	3
N_1	3000	3059	3340	3012
N_2	3000	3600	3600	3600
$\frac{C_{11}}{10^6}$ (H^{-1})	1.56	1.0358	0.87	1.2567
$\frac{C_{12}}{10^6}$ (H^{-1})	1.56	0.6	0.6	0.6
E_{tot} (J)	25,556	22,603	22,721	22,575

where rand(0,1) is a random number between zero and one. We developed the algorithm in MATLAB and captured many interesting results.

4 Results

The predetermined parameters given in Table 1 were obtained from the experimental work we have done for the single set as shown in Fig. 2. Figures 6–9 present the optimization process for the design variables utilizing the gradient based, genetic, and SA algorithms. The GS, genetic, and SA algorithms terminate after 8000, 1360, and 24,000 iterations, respectively, satisfying the tolerances defined for both the variables and the lumped cost function. All methods yield lower values of C_{11}, C_{12}, C_{21}, C_{22}, g_{m1}, and g_{m2}, and higher values for the number of coils with respect to their corresponding nominal values listed in Table 2

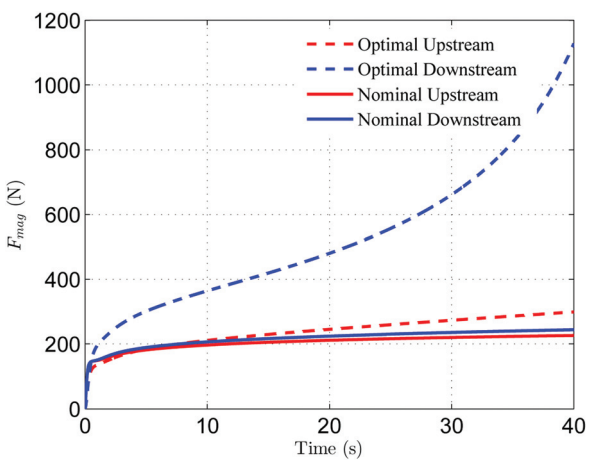

Fig. 10 The optimal and nominal magnetic forces

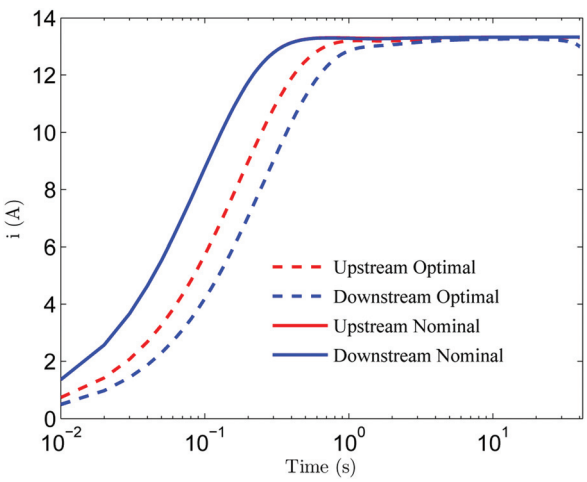

Fig. 11 The optimal and nominal applied currents

Downloaded From: http://mechanicaldesign.asmedigitalcollection.asme.org/ on 02/19/2016 Terms of Use: http://www.asme.org/about-asme/terms-of-use

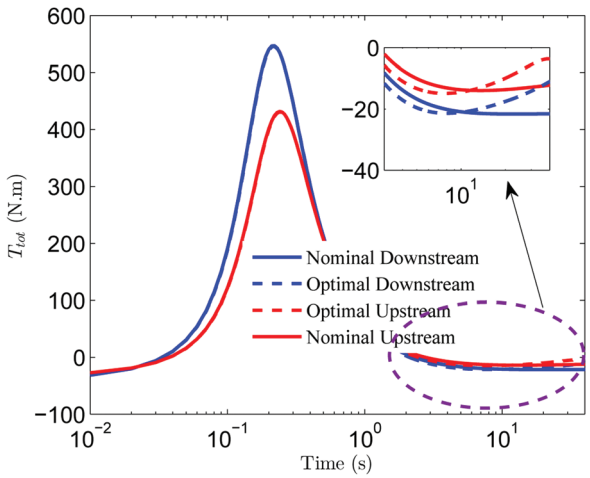

Fig. 12 The total torques acting on both the valves

$$\frac{T_{h2}}{T_{h1}} \propto \left(\frac{D_{v2}}{D_{v1}}\right)^3 \times \left(\frac{c_{v1}}{c_{v2}}\right)^2 \tag{38}$$

$$\frac{T_{b2}}{T_{b1}} \propto \left(\frac{D_{v2}c_{v1}}{D_{v1}c_{v2}}\right)^2 \tag{39}$$

These optimal variables to be used in the actuation parts are considerably more efficient in that higher and lower values of the actuation forces and currents are obtained as shown in Figs. 10 and 11, respectively. Note that, for both the nominal and optimal configurations, the downstream actuator's currents and forces are lower and higher, respectively, than those of the upstream ones, particularly for the optimal sets. This can be potentially explained as due to the sudden contraction between the valves. The change of pipe diameter would potentially yield higher values of both the hydrodynamic and bearing torques acting on the downstream valve based on Eqs. (7)–(9), (21), and (22).

The downstream set is hence expected, for both the nominal and optimal cases, to be subject to the higher hydrodynamic and bearing torques for the approximate ranges of $0 \leq \alpha_i \leq 60$ deg and $\alpha_i \geq 60$ deg [5], respectively, as shown in Fig. 12. From another aspect, we previously established the important roles of both the hydrodynamic and bearing torques on the valve motions. The hydrodynamic torque is a helping load to push the valve to be closed and is typically effective for when the valve angle is lower than 60 deg [6]. Note that the bearing torque is a resistance load and remarkably becomes effective for the valve's angle higher than that of 60 deg; we validated the effective ranges experimentally [6] which indicate the helping and resisting natures of the hydrodynamic and bearing torques by presenting positive and negative values, respectively. Consequently, the higher helping loads would lead to the downstream valve's higher rotation angles than those of the upstream ones, as shown in Fig. 13; $\alpha_{1no} = 22$ deg, $\alpha_{2no} = 26$ deg, $\alpha_{1op} = 63$ deg, and $\alpha_{2op} = 75$ deg. The higher rotation angles minimize the denominator of the magnetic force term stated in Eq. (25) and a slightly higher value of the force can be observed for the nominal downstream set and considerably higher amount for the optimal one.

The optimal design variables which include smaller values of C_{1i} 's, C_{2i} 's, g_m's and higher values of N_i's would also help magnify the magnetic forces based on Eq. (25). From another aspect, the circled area shown in Fig. 12 confirms the reduced bearing torques of the optimal sets compared to those of the nominal ones; this helps consume lower values of the currents leading to a lower energy consumption. Smaller amounts of currents are used in the optimal sets as shown in Fig. 11; this can be related to the decreased resistance torques (the bearing ones) in addition to the increased magnetic forces. Subsequently, we would be able to apply a lower level of the lumped energy to carry out the closing operation.

Consequently, reduced amounts of energies are consumed as shown in Figs. 14(*a*)–14(*c*). Figures 14(*a*)–14(*c*) reveal upward of 13.09%, 12.57%, and 13.22% energy savings obtained through the GS, genetic, and SA algorithms, respectively,

$$\Delta E_{\mathrm{GS}} = \frac{E_{\mathrm{nominal}} - E_{\mathrm{optimal}}}{E_{\mathrm{nominal}}} \times 100 \approx 13.09\% \tag{40}$$

$$\Delta E_{\mathrm{GA}} = \frac{E_{\mathrm{nominal}} - E_{\mathrm{optimal}}}{E_{\mathrm{nominal}}} \times 100 \approx 12.57\% \tag{41}$$

$$\Delta E_{\mathrm{SA}} = \frac{E_{\mathrm{nominal}} - E_{\mathrm{optimal}}}{E_{\mathrm{nominal}}} \times 100 \approx 13.22\% \tag{42}$$

We repeatedly examined the optimization schemes to avoid being trapped in local minima. The negligible difference (less than 0.65%) among the GS, genetic, and SA algorithms would potentially confirm the global minimum value which looks meaningful from the point of view of the physics of the system. The amount of energy saved is promising in which we typically run thousands of valve-actuator sets in a flow line and using such optimal configurations would help reduce the amount of energy consumption and subsequently the cost of operation for the whole network.

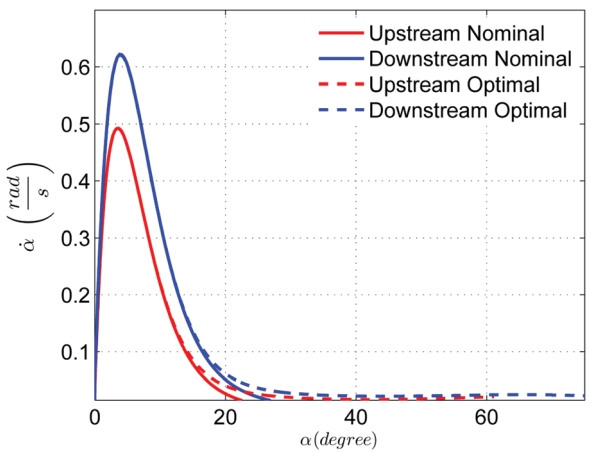

Fig. 13 The optimal and nominal valves' rotation angles

5 Conclusions

This paper presented a novel coupled nonlinear model of two actuators and valves subject to the sudden contraction. We discussed the effects of mutual interactions between the valves' dynamics in correlations with the flow nonlinear torques including both the hydrodynamic and bearing ones. These dependencies among different components were formalized to yield a sixth-order dynamic model of the whole system. We used SA, genetic, and gradient based algorithms to carry out optimization and obtain the global minimum of the cost function defined as the sum of energy consumed in each valve-actuator set.

The principal results of this paper can be summarized as follows:

- Energy can be saved by a significant amount (as much as 13%) by implementing optimal design.
- The optimal flow torques help consume a minimum level of the lumped energy.

Downloaded From: http://mechanicaldesign.asmedigitalcollection.asme.org/ on 02/19/2016 Terms of Use: http://www.asme.org/about-asme/terms-of-use

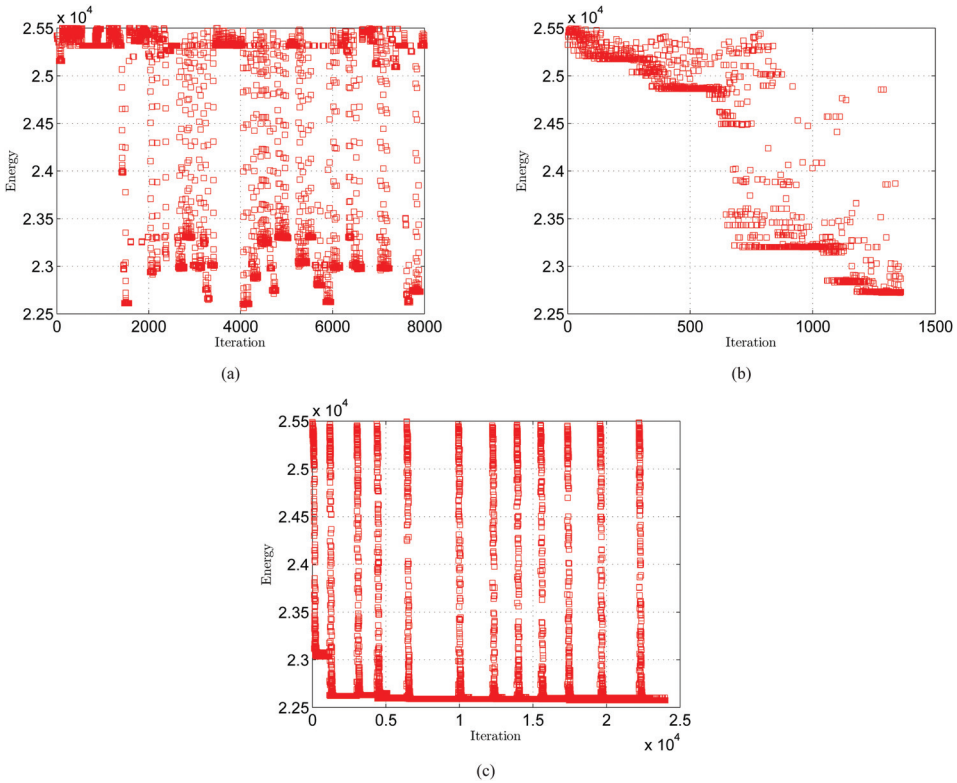

Fig. 14 The optimized lumped amount of energy: (*a*) GS ($E_{opm} = 22{,}603$), and (*b*) GA ($E_{opm} = 22{,}721$), and (*c*) SA ($E_{opm} = 22{,}557$)

- Lower values of the currents and subsequently instantaneous energies (by plotting $E_{ins} = v_i i_i$ versus α_i) are consumed particularly for higher rotation angles.
- Higher values of the motive forces are obtained.

We are currently focusing our efforts on developing a comprehensive model for n valves and actuators to be operated optimally in series.

Acknowledgment

The experimental work of this research was supported by Office of Naval Research Grant (No. N00014/2008/1/0435). We appreciate this grant and the advice and direction provided by Mr. Anthony Seman III, the program manager.

Nomenclature

A_d = area of valve's disk
b_{di} = equivalent damping coefficient of ith valve
C_i = constant coefficient of bearing torque acting on ith valve
C_{ii} = magnetic reluctances of ith actuator
c_{vi} = ith valve's coefficient
D_{si} = stem diameter of ith valve
D_{vi} = diameter of ith valve
E_{tot} = lumped amount of energy
F_{mi} = magnetic force of ith actuator
g_{mi} = airgap of ith actuator
i_i = current of ith actuator
J_i = polar moment of inertia of ith valve
k_i = equivalent stiffness
K_{con} = coefficient of pressure drop due to pipe contraction
L_i = pipe length before and after pipe contraction
N_i = number of coils of ith actuator
P_{coni} = pressure before and after pipe contraction
P_{in} = inlet pressure
P_{out} = outlet pressure
P_1 = pressure after upstream valve
P_2 = pressure before downstream valve
q_v = volumetric flow rate
q_{in} = inlet volumetric flow rate
q_{out} = outlet volumetric flow rate
R_i = coil electrical resistance of ith actuator
r_i = radius of ith pinion
R_{con} = resistance due to pipe contraction
R_{Li} = resistance due to head loss before and after pipe contraction
R_{ni} = changing resistance of ith valve
t_f = nominal operation time
T_{bi} = bearing torque acting on ith valve
T_{hi} = hydrodynamic torque acting on ith valve
v = flow mean velocity
V_i = voltage of ith actuator
v_{out} = outlet flow velocity
x_i = linear displacement of ith plunger
$\dot{x}_i$ = linear velocity of ith plunger
z_i = state variable
α_i = rotation angle of ith valve
$\dot{\alpha}_i$ = angular velocity of ith valve
β = ratio of minor and major diameters
θ = angle of approach
θ_1 = lumped design variables
μ = friction coefficient between bearing area and valve's stem
μ_f = fluid dynamic viscosity
ρ = density of media

References

[1] Hughes, R., Balestrini, S., Kelly, K., Weston, N., and Mavris, D., 2006, "Modeling of an Integrated Reconfigurable Intelligent System (IRIS) for Ship Design," 2006 ASNE Ship and Ship Systems Technology (S3T) Symposium.
[2] Lequesne, B., Henry, R., and Kamal, M., 1998, "Magnavalve: A New Solenoid Configuration Based on a Spring-Mass Oscillatory System for Engine Valve Actuation," GM Research Report No. E3-89.

Downloaded From: http://mechanicaldesign.asmedigitalcollection.asme.org/ on 02/19/2016 Terms of Use: http://www.asme.org/about-asme/terms-of-use

[3] Naseradinmousavi, P., and Nataraj, C., 2011, "Nonlinear Mathematical Modeling of Butterfly Valves Driven by Solenoid Actuators," J. Appl. Math. Modell., **35**(5), pp. 2324–2335.
[4] Naseradinmousavi, P., and Nataraj, C., 2012, "Transient Chaos and Crisis Phenomena in Butterfly Valves Driven by Solenoid Actuators," Commun. Nonlinear Sci. Numer. Simul., **17**(11), pp. 4336–4345.
[5] Naseradinmousavi, P., and Nataraj, C., 2013, "Optimal Design of Solenoid Actuators Driving Butterfly Valves," ASME J. Mech. Des., **135**(9), p. 094501.
[6] Naseradinmousavi, P., 2015, "A Novel Nonlinear Modeling and Dynamic Analysis of Solenoid Actuated Butterfly Valves Coupled in Series," ASME J. Dyn. Syst., Meas., Control, **137**(1), p. 014505.
[7] Belato, D., Weber, H. I., Balthazar, J. M., and Mook, D. T., 2001, "Chaotic Vibrations of a Nonideal Electro-Mechanical System," Int. J. Solids Struct., **38**(10–13), pp. 1699–1706.
[8] Xie, W. C., Lee, H. P., and Lim, S. P., 2003, "Nonlinear Dynamic Analysis of MEMS Switches by Nonlinear Modal Analysis," J. Nonlinear Dyn., **31**(3), pp. 243–256.
[9] Boivin, N., Pierre, C., and Shaw, S. W., 1995, "Non-Linear Normal Modes, Invariance, and Modal Dynamics Approximations of Non-Linear Systems," J. Nonlinear Dyn., **8**(3), pp. 315–346.
[10] Ge, Z. M., and Lin, T. N., 2003, "Chaos, Chaos Control and Synchronization of Electro-Mechanical Gyrostat System," J. Sound Vib., **259**(3), pp. 585–603.
[11] Baek-Ju, S., and Eun-Woong, L., 2005, "Optimal Design and Speed Increasing Method of Solenoid Actuator Using a Non-Magnetic Ring," International Conference on Power Electronics and Drives Systems (PEDS), pp. 1140–1145.
[12] Hameyer, K., and Nienhaus, M., 2002, "Electromagnetic Actuator-Current Developments and Examples," 8th International Conference on New Actuators, pp. 170–175.
[13] Sung, B. J., Lee, E. W., and Kim, H. E., 2002, "Development of Design Program for On and Off Type Solenoid Actuator," KIEE Summer Annual Conference, Vol. B, pp. 929–931.
[14] Kajima, T., 1995, "Dynamic Model of the Plunger Type Solenoids at Deenergizing State," IEEE Trans. Magn., **31**(3), pp. 2315–2323.
[15] Scott, D. A., Karr, C. L., and Schinstock, D. E., 1999, "Genetic Algorithm Frequency-Domain Optimization of an Anti-Resonant Electromechanical Controller," *Eng. Appl. Artificial Intell.*, **12**(2), pp. 201–211.
[16] Mahdi, S. A., 2014, "Optimization of PID Controller Parameters Based on Genetic Algorithm for Non-Linear Electromechanical Actuator," Int. J. Comput. Appl., **94**(3), pp. 11–20.
[17] Jimenez-Octavio, J. R., Pil, E., Lopez-Garcia, O., and Carnicero, A., 2006, "Coupled Electromechanical Cost Optimization of High Speed Railway Overheads," ASME Paper No. JRC2006-94023.
[18] Nowak, L., 2010, "Optimization of the Electromechanical Systems on the Basis of Coupled Field-Circuit Approach," Int. J. Comput. Math. Electr. Electron. Eng., **20**(1), pp. 39–52.
[19] Marquardt, D., 1963, "An Algorithm for Least-Squares Estimation of Nonlinear Parameters," SIAM J. Appl. Math., **11**(2), pp. 431–441.
[20] Messine, F., Nogarede, B., and Lagouanelle, J. L., 1998, "Optimal Design of Electromechanical Actuators: A New Method Based on Global Optimization," IEEE Trans. Magn., **34**(1), pp. 299–308.
[21] Kelley, C. T., 1999, "Iterative Methods for Optimization," *Frontiers in Applied Mathematics*, Vol. 18, SIAM, Philadelphia, PA.
[22] Sefkat, G., 2009, "The Design Optimization of the Electromechanical Actuator," Struct. Multidiscip. Optim., **37**(6), pp. 635–644.
[23] Abergel, J., Allain, M., Michaud, H., Cueff, M., Ricart, T., Dieppedale, C., Rhun, G. L., Faralli, D., Fanget, S., and Defay, E., 2012, "Optimized Gradient-Free PZT Thin Films for Micro-Actuators," 2012 IEEE International Ultrasonics Symposium (IUS), Dresden, Germany, Oct. 7–10, pp. 972–974.
[24] Chakraborty, I., Trawick, D. R., Jackson, D., and Mavris, D., 2013, "Electric Control Surface Actuator Design Optimization and Allocation for the More Electric Aircraft," AIAA Paper No. 2013-4283.
[25] Medhat, A., and Youssef, M., 2013, "Optimized PID Tracking Controller for Piezoelectric Hysteretic Actuator Model," World J. Modell. Simul., **9**(3), pp. 223–234.
[26] Naseradinmousavi, P., 2012, "Nonlinear Modeling, Dynamic Analysis, and Optimal Design and Operation of Electromechanical Valve Systems," Ph.D. thesis, Villanova University, Villanova, PA.
[27] Bennett, C. O., and Myers, J. E., 1962, *Momentum, Heat, and Mass Transfer*, McGraw-Hill, New York.
[28] Massey, B. S., and Ward-Smith, J., 1998, *Mechanics of Fluids*, 7th ed., Taylor & Francis, London/New York.
[29] American Water Works Association, 2012, *Butterfly Valves: Torque, Head Loss, and Cavitation Analysis*, 2nd ed., AWWA, Denver, CO.
[30] Park, J. Y., and Chung, M. K., 2006, "Study on Hydrodynamic Torque of a Butterfly Valve," ASME J. Fluids Eng., **128**(1), pp. 190–195.
[31] Leutwyler, Z., and Dalton, C., 2008, "A CFD Study of the Flow Field, Resultant Force, and Aerodynamic Torque on a Symmetric Disk Butterfly Valve in a Compressible Fluid," ASME J. Pressure Vessel Technol., **130**(2), p. 021302.
[32] Naseradinmousavi, P., and Nataraj, C., 2011, "A Chaotic Blue Sky Catastrophe of Butterfly Valves Driven by Solenoid Actuators," ASME Paper No. IMECE2011/62608.
[33] Kirkpatrick, S., Gelatt, C. D., and Vecchi, M. P., 1983, "Optimization by Simulated Annealing," Science, **220**(4598), pp. 671–680.
[34] Cerny, V., 1985, "Thermodynamical Approach to the Traveling Salesman Problem: An Efficient Simulation Algorithm," J. Optim. Theory Appl., **45**(1), January, **45**(1), pp. 41–55.
[35] Holland, H. J., 1975, *Adaptation in Natural and Artificial Systems*, University of Michigan Press, Ann Arbor, MI.

Downloaded From: http://mechanicaldesign.asmedigitalcollection.asme.org/ on 02/19/2016 Terms of Use: http://www.asme.org/about-asme/terms-of-use